J. Phys. B: At. Mol. Opt. Phys. 27 (1994) 5065–5081. Printed in the UK

Hyperspherical close-coupling calculation of positronium formation cross sections in positron–hydrogen scattering at low energies

Yan Zhou and C D Lin
Department of Physics, Kansas State University, Manhattan, KS 66506, USA

Received 11 February 1994, in final form 23 August 1994

Abstract. The hyperspherical close-coupling method is applied to calculate both the elastic and positronium formation cross sections for positron collisions with atomic hydrogen at low energies. By treating the hyperradius as a slow variable, the Schrödinger equation in the body frame at each fixed hyperradius is solved using the higher-order finite-element method and the resulting hyperradial equations are solved using the diabatic-by-sector method. The coupled hyperradial equations are integrated to a large hyperradius where the wavefunctions are matched to the known asymptotic solutions to extract the scattering matrix. Both the elastic and the positronium formation cross sections are calculated at energies below the H($n = 2$) excitation threshold for $J = 0$, 1, 2 and 3. It is shown that the present hyperspherical close coupling method gives results comparable to those obtained by elaborate variational methods.

1. Introduction

In recent years the development of intense positron sources and the improvement in experimental techniques have made it possible to measure directly the positronium formation cross sections in positron collisions with atoms (DeVries *et al* 1993, Kwan *et al* 1993 and references in Humberston 1986, Humberston and Armour 1987). While measurements for the scattering of positrons by atomic hydrogen are not available except at higher energies (Sperber *et al* 1992, Zhou *et al* 1993b, Stein *et al* 1993), this subject has been studied extensively by many theoretical methods over the years. On the one hand, it is interesting to examine the difference between the scattering of an atomic hydrogen by electrons and by positrons. For electron–hydrogen collisions, the indistinguishability between the incident and target electrons imposes symmetry boundary conditions which are not required for positron–hydrogen collisions. On the other hand, collisions between positrons and atomic hydrogen can result in the formation of positronium where the electron and positron combine to form a bound composite system. Theoretically the description of rearrangement collisions is much more difficult, and thus calculations of positronium formation cross section have been of much interest.

The positronium formation cross sections have been studied over the years using many theoretical methods. Most of the calculations are concentrated in the so-called Ore gap region, i.e., the energy region between the formation of the positronium ground state and the first excited state of atomic hydrogen (total energy between −0.25 au and −0.125 au). Besides the simple perturbative theories which are not expected to be valid at the low energies considered here, there have been three major theoretical approaches. The first and often considered to be the most accurate is based on the Kohn variational principle.

0953-4075/94/205065+17$19.50

Such calculations have been carried out for $J = 0$, 1 and 2 (Brown and Humberston 1985, Humberston 1986). These calculations are rather elaborate and the variational parameters have to be determined at each energy and for each partial wave. The second approach is based on the close coupling method where the wavefunction of the collision system is expanded in terms of bound states (and sometimes pseudostates also) of atomic hydrogen and of the positronium (Basu *et al* 1989, Hewitt *et al* 1990, Liu and Gien 1992, Mitroy 1993). In the close coupling calculations the importance of pseudostates is difficult to evaluate.

An alternative method for treating rearrangement collisions has been formulated using hyperspherical coordinates since the 1960s in connection with chemical reactive scattering (Smith 1960) and in collisions involving nucleons (Delves 1959, 1962). In recent years great progress has been made, in particular, in the calculation of atom–diatom reactive scattering cross sections. There are several quantum chemistry groups where the reactive scatterings such as $H + D_2 \rightarrow HD + D$ or $F + H_2 \rightarrow FH + H$ were studied (Launay and Le Dourneuf 1989, Launay 1990). Despite the great success of such studies, the utilities of the hyperspherical approach have not been critically tested. First, in chemical reactive scatterings the interatomic potentials can be determined only approximately, either by *ab initio* calculations or by semi-empirical fitting of spectroscopic data, which thus limit the accuracy of the results obtained. Second, the number of rotational and vibrational levels of a molecule is quite large within a narrow energy range such that calculations always have to be carried out by including a large number of rovibrational excited states. Analysis and understanding of results from such large scale calculations are more difficult.

In atomic physics, the hyperspherical coordinates have been used in the last two decades in the classification of doubly excited states of atoms (Lin 1984, 1986). Recently, it has been further extended to general Coulomb three-body systems where the masses of the particles are arbitrary (Lin and Liu 1988, Chen and Lin 1990, Liu *et al* 1991, Zhou *et al* 1993c). These studies provided the qualitative understanding of the Coulombic systems and the variation of the properties of these systems with the masses was examined. In the meanwhile, numerical improvement has been made in the last few years such that the hyperspherical close coupling (HSCC) method has now been applied routinely to atomic systems, including accurate calculations of resonance energies, resonance widths and photoionization spectra (Tang *et al* 1992a, Zhou *et al* 1993a). It has been shown that results from the HSCC method are as accurate as those obtained by variational methods and the computational efforts required are much less than other methods. Thus the HSCC method has been used to calculate photoabsorption spectra for higher doubly excited states where many channels are open (Tang *et al* 1992b).

The present paper describes the extension of the HSCC method to arbitrary three-body systems. In particular, we will concentrate on the calculation of elastic and the positronium formation cross sections in the Ore gap region. However, the method is quite general, and it is being extended to collisions at higher energies and to other collision systems.

The HSCC method has been applied previously to positron–atomic hydrogen scattering by Archer *et al* (1990) where they employed 40 channels in the inner region and the wavefunctions are matched at $R = 120$. Their hyperangles are defined differently from ours and they solved the two-dimensional partial differential equations using the finite-element method where the wavefunction in each element is expanded in terms of a product of second-order polynomials. We used fifth-order polynomials to expand the wavefunction in each element (Zhou *et al* 1993c) and can achieve higher numerical accuracy for the potential curves. Furthermore, Archer *et al* applied the method only to the case where the total orbital angular momentum is zero. Very recently another calculation which is very

similar to ours has been carried out by Igarashi and Toshima (1994). They used the same hyperspherical coordinates, but the wavefunctions were calculated in the laboratory-fixed frame and the potential curves are calculated using Slater orbitals of the positronium and the atomic hydrogen. We differ from them mostly in the numerical details.

In this paper we describe in detail the application of the HSCC method to the collisions of a three-body system. The relevant equations and the numerical approaches are described in section 2. The calculated elastic scattering and the positronium formation cross sections for positron–atomic hydrogen collision are given in section 3. A summary and discussion of future developments are given in section 4. Atomic units are used unless otherwise noted.

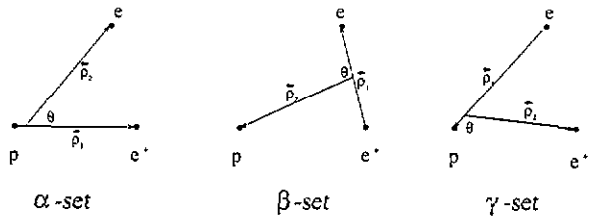

Figure 1. Definition of the three sets of Jacobi coordinates for the $e^+ + H$ collision system.

2. The hyperspherical close coupling approach

2.1. Summary of the hyperspherical coordinates

For the positron–hydrogen atom system, three sets, (α, β, γ), of internal Jacobi coordinates can be defined, see figure 1.

For each set of Jacobi coordinates, one can define two mass-weighted vectors

$$\xi_1 = \sqrt{\frac{\mu_1}{\mu}}\rho_1 \qquad \xi_2 = \sqrt{\frac{\mu_2}{\mu}}\rho_2 \tag{1}$$

where μ_1 and μ_2 are the reduced masses associated with each vector ρ_1 and ρ_2. The parameter μ is an arbitrary scaling factor which is set to be $\mu = (m_p + m_e)/m_p m_e \approx 1$. For each set of Jacobi coordinates, a hyperspherical radius R and a hyperangle ϕ are defined as

$$R^2 = \xi_1^2 + \xi_2^2 \qquad \tan\phi = \xi_2/\xi_1 \tag{2}$$

where R^2 is propotional to the moment of inertia of the system, and is invariant with respect to the three sets of Jacobi coordinates.

After introducing the reduced wavefunction

$$\Psi(R, \phi, \hat{\Omega}) = \psi R^{5/2} \sin\phi \cos\phi \tag{3}$$

(ψ is the whole wavefunction), the Schödinger equation is of the form

$$\left(-\frac{\partial^2}{\partial R^2} + H_{ad} - 2\mu E\right)\Psi(R, \phi, \hat{\Omega}) = 0 \tag{4}$$

where $\hat{\Omega}$ denotes collectively the four orientation angles of vectors ρ_1 and ρ_2. The adiabatic Hamiltonian is

$$H_{\rm ad}(R;\phi,\hat{\Omega}) = \frac{\Lambda^2 + 2\mu RC(\phi,\theta)}{R^2} \tag{5}$$

with

$$\Lambda^2 = \left(-\frac{\partial^2}{\partial\phi^2} + \frac{l_1^2}{\cos^2\phi} + \frac{l_2^2}{\sin^2\phi}\right) - \frac{1}{4} \tag{6}$$

where l_1 and l_2 are the usual orbital angular mometum operators, and

$$C(\phi,\theta) = \sqrt{\frac{\mu_1^\alpha}{\mu}}\frac{Z_1Z_2}{\cos\phi^\alpha} + \sqrt{\frac{\mu_1^\beta}{\mu}}\frac{Z_2Z_3}{\cos\phi^\beta} + \sqrt{\frac{\mu_1^\gamma}{\mu}}\frac{Z_3Z_1}{\cos\phi^\gamma} \tag{7}$$

is the effective charge among the three particles. In (7), Z_i is the charge of particle i, and the hyperangle in each set of Jacobi coordinates has been explicitly given. The angles ϕ,θ on the left can be angles in any one of the three Jacobi sets.

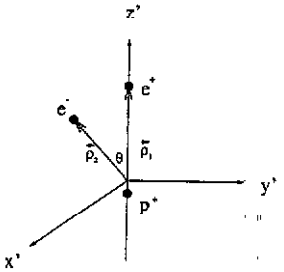

Figure 2. Body-frame axes. The three particles lie on the x'–z' plane with the z' axis along the proton–positron line and the electron above the x'–y' plane.

2.2. *Expansion of wavefunctions in the body frame*

The coordinate system in the body frame is defined as in figure 2 where the quantization axis is along the line joining the proton and the positron and the three particles lie on the $x'z'$ plane. After some elaborate algebra, the Λ^2 operator takes the form

$$\Lambda^2 = T_0 + T_1 + T_2 - \tfrac{1}{4} \tag{8}$$

where

$$T_0 \equiv -\frac{\partial^2}{\partial\phi^2} - \frac{1}{\sin^2\phi\cos^2\phi\sin\theta}\frac{\partial}{\partial\theta}\left(\sin\theta\frac{\partial}{\partial\theta}\right) \tag{9}$$

$$T_1 \equiv \frac{\hat{l}_{z'}^2}{\sin^2\phi\cos^2\phi\sin^2\theta} - \frac{2l_{z'}^2 - J^2}{\cos^2\phi} \tag{10}$$

$$T_2 \equiv \left(2i\hat{l}_{y'}\frac{\partial}{\partial\theta} + 2\cot\theta\hat{l}_{x'}\hat{l}_{z'}\right)/\cos^2\phi \tag{11}$$

and the angular momentum operators with respect to the body-frame axes are

$$\hat{l}_{x'} = -\mathrm{i}\left(\sin\omega_3\frac{\partial}{\partial\omega_2} - \frac{\cos\omega_3}{\sin\omega_2}\frac{\partial}{\partial\omega_1} + \cot\omega_2\cos\omega_3\frac{\partial}{\partial\omega_3}\right) \tag{12}$$

$$\hat{l}_{y'} = -\mathrm{i}\left(\cos\omega_3\frac{\partial}{\partial\omega_2} + \frac{\sin\omega_3}{\sin\omega_2}\frac{\partial}{\partial\omega_1} - \cot\omega_2\sin\omega_3\frac{\partial}{\partial\omega_3}\right) \tag{13}$$

$$\hat{l}_{z'} = -\mathrm{i}\frac{\partial}{\partial\omega_3} \tag{14}$$

where ω_1, ω_2, ω_3 are the three Euler angles of the body-frame axes with respect to the space-fixed frame (Landau and Lifshitz 1977).

From the definition of the operators, T_0 and T_1 are diagonal with respect to the magnetic components l along the z' axis of the body-frame and T_2 operator couples only states with adjacent l components. Note that T_2 is similar to the rotational coupling in atomic collisions.

The wavefunction which describes the overall rotation of the three-body system can be separated out. Define the normalized and symmetrized D-functions associated with our choice of the body-frame (Bhatia and Temkin 1964)

$$\tilde{D}^J_{lM_J}(\omega_1,\omega_2,\omega_3) = \frac{\sqrt{2J+1}}{4\pi\left[1+(\sqrt{2}-1)\delta_{l0}\right]}\left[D^J_{lM_J} + (-1)^{l+J}PD^J_{-lM_J}\right] \tag{15}$$

which are eigenfunctions of operators J^2,J_z,$l^2_{z'}$ and parity. Here P is the parity, J is the total angular momentum, l is the absolute value of the projection of J along the body frame's z' axis and M_J is the projection along the space-fixed z axis. If $(-1)^J P = 1$, l runs from 0 to J; if $(-1)^J P = -1$, l runs from 1 to J.

2.3. The diabatic-by-sector approach

In the so-called diabatic-by-sector approach, the reduced wavefunction Ψ is expanded in terms of $\tilde{D}$ and the diabatic-by-sector bases $\Phi_{\mu l}(R_a;\theta,\phi)$:

$$\Psi(R,\phi,\hat{\Omega}) = \sum_{\mu}\sum_{l} F_{\mu l}(R)\Phi_{\mu l}(R_a;\theta,\phi)\tilde{D}^J_{lM_J}(\omega_1,\omega_2,\omega_3). \tag{16}$$

In contrast to the standard adiabatic approach or the Born–Oppenheimer approximation, the diabatic-by-sector bases are defined only at discretized values of R. In this approach the hyperradius is divided into many small sectors. Within each sector, the base function, $\Phi_{\mu l}(R_a;\theta,\phi)$, is fixed where R_a is often chosen to be at the midpoint of each sector. Since the base functions are fixed within each sector, $(\partial/\partial R)\Phi_{\mu l}(R_a;\theta,\phi) = 0$, and thus the basis functions are diabatic. The diabatic functions $\Phi_{\mu l}$ are chosen to satisfy

$$\left[\frac{T_0 + \langle\tilde{D}^J_{lM_J}|T_1|\tilde{D}^J_{lM_J}\rangle}{R_a^2} + \frac{2\mu C}{R_a}\right]\Phi_{\mu l}(R_a;\theta,\phi) = 2\mu U_{\mu l}(R_a)\Phi_{\mu l}(R_a;\theta,\phi) \tag{17}$$

with $0 \leqslant \theta \leqslant \pi$ and $0 \leqslant \phi \leqslant \frac{1}{2}\pi$. Here

$$\langle\tilde{D}^J_{lM_J}|T_1|\tilde{D}^J_{lM_J}\rangle = \frac{l^2}{\sin^2\phi\cos^2\phi\sin^2\theta} + \frac{J(J+1)-2l^2}{\cos^2\phi}. \tag{18}$$

Within the sector, the hyperradial functions $F_{\mu I}$ then satisfy the coupled differential equations

$$\left(-\frac{\partial^2}{\partial R^2}-\frac{1}{4R^2}-2\mu E\right)F_{\mu I}(R)+\sum_{\nu I'}V_{\mu I,\nu I'}(R)F_{\nu I'}(R)=0 \tag{19}$$

where

$$V_{\mu I,\nu I'}(R)=\langle\Phi_{\mu I}(R_a;\theta,\phi)\tilde{D}^J_{IM_J}|\frac{T_0+T_1+T_2}{R^2}+\frac{2\mu C}{R}|\Phi_{\nu I'}(R_a;\theta,\phi)\tilde{D}^J_{I'M_J}\rangle \tag{20}$$

and E is the total energy of the system in the centre-of-mass frame.

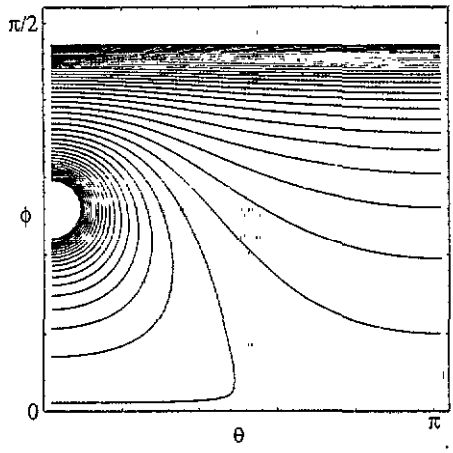

Figure 3. Contour plot of the potential surface of the $e^+ + H$ system on the $(\theta^\alpha, \phi^\alpha)$ plane. Two potential valleys occur at $(\theta^\alpha, \phi^\alpha) = (0°, 45°)$ and $(180°, 0.0311°)$, respectively. The latter is not clearly visible on the plot since it is very close to the right lower corner of the frame.

2.4. Numerical calculations of the diabatic basis functions

One of the major numerical difficulties in the present approach is the accurate solution of the partial differential equation (17). To ensure that the excitation of atomic hydrogen and the positronium formation channels are treated on equal footing, we solve equation (17) in the α-set coordinates. In this coordinate system, the effective charge C on the (θ, ϕ) plane exhibits two singularities, as shown in figure 3. The first singularity can be easily seen to occur at $\theta = 0°$, $\phi = 45°$, and the other singularity occurs at $\theta = 180°$, $\phi = 0.0311°$ which is very close to the lower right-hand corner and is not clearly seen in the contour plot in figure 3.

We solve the two-dimensional partial differential equation (17) using the finite-element method (FEM) (Bathe and Wilson, 1976). The (θ, ϕ) plane is divided into 240 rectangular elements, 10 in θ, and 24 in ϕ. At large hyperradius, the wavefunctions are localized near the singular points of one or the other potential valley of figure 3. To account for these localizations, we choose the elements in such a way that more elements are used near the singular points. In each element, $\Phi_{\mu I}$ is expanded in 36 local bases (see, for example, Shertzer and Levin 1991, Zhou *et al* 1993a, b, c), each of which is a product of two fifth-order polynomials of θ and ϕ, respectively. The expansion coefficients are the values of

$\Phi_{\mu I}$, $\partial\Phi_{\mu I}/\partial\phi$, $\partial\Phi_{\mu I}/\partial\theta$ and $\partial^2\Phi_{\mu I}/\partial\phi\partial\theta$ at the nine nodes of the element which are the four points at the corners, four at the midpoint of each side and another at the centre of the rectangle. With this choice the size of the matrix is 4032. Since it is a sparse matrix, a special 'skyline' storage mode is used, and the subspace iteration method is utilized to calculate the lowest few ($\leqslant 20$) eigenvalues and the corresponding eigenfunctions.

The numerical accuracy depends on the number of elements used, and the eigenvalues are expected to be less accurate at large R where the wavefunctions are more localized near the singular points. However, even with the chosen 240 elements, we can achieve better than four-digit accuracy for the lowest eigenvalues which are expected to be the least accurate at large R because these wavefunctions are more localized. For instance, at $R_a = 29.93$, the calculated lowest $U_{\mu 0}$ for $J = 0$ is -1.0005423, while the eigenvalue obtained from the asymptotic expansion formula (Cavagnero *et al* 1990) gives $-1.000558 + O(1/R^4)$. At this R, the higher eigenvalues are expected to be more accurate since they are less localized. Similarly the eigenvalues at smaller R are expected to be more accurate. The accuracy of the eigenvalues obtained in this work is much improved from the calculations of Archer *et al* (1990). The latter group used second-order polynomials to expand the wavefunctions in each element and they can achieve only two-digit accuracy in eigenvalues at large R. In the present work the FEM calculations were carried out using the resources of Cornell Supercomputer Center.

2.5. *Evaluation of coupling matrix elements* $V_{\mu I,\nu I'}(R)$

From the definition, equations (9) and (10), the matrix element of $T_0 + T_1$ between channels with different I is zero, while the matrix element of T_2 is non-zero only for $I' = I \pm 1$. Furthermore

$$\begin{aligned}
&\langle \Phi_{\mu I}(R_a;\theta,\phi)\tilde{D}^J_{IM_J}|\frac{T_0+T_1}{R^2}+\frac{2\mu C}{R}|\Phi_{\nu I'}(R_a;\theta,\phi)\tilde{D}^J_{I'M_J}\rangle \\
&\quad=\langle \Phi_{\mu I}(R_a;\theta,\phi)\tilde{D}^J_{IM_J}|\frac{T_0+T_1}{R_a^2}\frac{R_a^2}{R^2}+\frac{2\mu C}{R}|\Phi_{\nu I'}(R_a;\theta,\phi)\tilde{D}^J_{I'M_J}\rangle \\
&\quad=\langle \Phi_{\mu I}(R_a;\theta,\phi)\tilde{D}^J_{IM_J}|2\mu(U_{I'\nu}-\frac{C}{R_a})\frac{R_a^2}{R^2}+\frac{2\mu C}{R}|\Phi_{\nu I'}(R_a;\theta,\phi)\tilde{D}^J_{I'M_J}\rangle \\
&\quad=\frac{2\mu}{R^2}\left[R_a^2 U_{I\mu}(R_a)\delta_{\mu\nu}+(R-R_a)C_{\mu\nu I}\right]\delta_{II'} \qquad (21)
\end{aligned}$$

and

$$\begin{aligned}
&\langle \Phi_{\mu I}(R_a;\theta,\phi)\tilde{D}^J_{IM_J}|T_2|\Phi_{\nu I'}(R_a;\theta,\phi)\tilde{D}^J_{I'M_J}\rangle \\
&\quad=\langle \Phi_{\mu I}(R_a;\theta,\phi)|h_{II+1}|\Phi_{\nu I+1}(R_a;\theta,\phi)\rangle\delta_{I'I+1} \\
&\qquad+\langle \Phi_{\mu I}(R_a;\theta,\phi)|h_{II-1}|\Phi_{\nu I-1}(R_a;\theta,\phi)\rangle\delta_{I'I-1} \qquad (22)
\end{aligned}$$

with

$$\begin{aligned}
C_{\mu\nu I} &= \langle \Phi_{\mu I}(R_a)|C|\Phi_{\nu I}(R_a)\rangle \\
h_{II\pm1} &= \frac{\gamma^J_{II\pm1}}{\cos^2\phi}\left(\pm\frac{\partial}{\partial\theta}+(I\pm1)\cot\theta\right) \\
\gamma^J_{II+1} &= -\left[1+(\sqrt{2}-1)\delta_{I0}\right][(J+I+1)(J-I)]^{1/2} \\
\gamma^J_{II-1} &= -\left[1+(\sqrt{2}-1)\delta_{I1}\right][(J-I+1)(J+I)]^{1/2}. \qquad (23)
\end{aligned}$$

Thus $V_{\mu I,\nu I'}(R)$ is given explicitly by

$$V_{\mu I,\nu I'}(R) = \frac{2\mu}{R^2}\left[R_a^2 U_{I\mu}\delta_{\mu\nu} + (R - R_a)C_{\mu\nu I}\right]\delta_{II'} + \frac{1}{R^2}\left[\langle\Phi_{\mu I}(R_a)|h_{II+1}|\Phi_{\nu I+1}(R_a)\rangle\delta_{I'I+1} + \langle\Phi_{\mu I}(R_a)|h_{II-1}|\Phi_{\nu I-1}(R_a)\rangle\delta_{I'I-1}\right]. \tag{24}$$

These matrix elements are identical to those derived by Kadomstsev and Vinitsky (1987) except that our ϕ is half of theirs.

2.6. Matching of inner region solutions and the asymptotic solutions

In this work we have divided the hyperradius into 267 sectors between $R = 0.03$ and $R = 29.93$. Starting with the smallest R with appropriate initial conditions, the coupled hyperradial equations (19) are integrated within the first sector. To propagate from one sector to the next, we need to calculate the transformation matrix $\langle\Phi_{\mu I}(R_a)|\Phi_{\nu I}(R_b)\rangle$, where R_a and R_b are chosen at the midpoint of each sector. The sector size is determined such that this transformation matrix remains unitary to about one part per 10^4. This procedure is repeated until a large value of R_0 is reached where the wavefunction is matched to the wavefunction in the asymptotic region. In the present calculation the R_0 is set at 29.93. At this boundary, the integrated solution from the inner region $\sum_{\mu I} F_{\mu I}(R_0)\Phi_{\mu I}(R_0;\theta,\phi)\tilde{D}^J_{IM_J}(\omega_1,\omega_2,\omega_3)$ is matched to the wavefunction in the asymptotic region where the three-body system is either dissociated to a hydrogen atom and a positron or a positronium and a proton. The asymptotic wavefunction $\psi_A^{(\lambda)}$ of the dissociated system can be represented by

$$\psi_A^{(\lambda)}(\rho_1,\rho_2) = \sum_{i=1}^{N} \frac{\varphi_i(\rho_1^\tau)\mathcal{Y}_{l_1^\tau l_2^\tau JM_J}(\hat{\Omega}_1^\tau,\hat{\Omega}_2^\tau)\left[f_\lambda(\rho_2^\tau)\delta_{i\lambda} - g_i(\rho_2^\tau)K_{i\lambda}\right]}{\rho_1^\tau\rho_2^\tau} \tag{25}$$

where $\varphi_i(\rho_1^\tau)$ are the bound state hydrogenic functions if τ denotes the γ-set coordinates which are suitable for describing the excitation of atomic hydrogen, or bound states of the positronium if τ refers to β-set coordinates for describing positronium formation channels. In the equation, f and g are velocity-normalized regular and irregular spherical Bessel functions $\frac{1}{\sqrt{v^\tau}}j_{l_2^\tau}$ and $\frac{1}{\sqrt{v^\tau}}n_{l_2^\tau}$, respectively, with v^τ as the relative velocity of the particle pair and the far-away particle of the τ arrangement, $K_{i\lambda}$ is the element of the K matrix, and the $\mathcal{Y}$ are the coupled angular momentum functions. The matching of the two solutions at R_0 becomes

$$\frac{1}{R_0^{5/2}\sin\phi\cos\phi}\sum_{\sigma=1}^{N} H_\sigma^\lambda \Psi^{(\sigma)}(R_0,\phi,\hat{\Omega}) = \psi_A^{(\lambda)}(\rho_1,\rho_2)\,|_{R=R_0} \tag{26}$$

with H_σ^λ being the expansion coefficients.

The asymptotic wavefunction $\psi_A^{(\lambda)}(\rho_1,\rho_2)$ as given in equation (25) is expressed in the laboratory-fixed frame. To solve equation (26), one needs to expand it by referring to the body frame. Note that

$$\mathcal{Y}_{l_1^\tau l_2^\tau JM_J}(\hat{\Omega}_1^\tau,\hat{\Omega}_2^\tau) = \sqrt{\frac{16\pi^2}{2J+1}}\sum_{I}^{J}\frac{\tilde{D}^J_{IM_J}(\omega_1,\omega_2,\omega_3)}{1+(\sqrt{2}-1)\delta_{I0}}\mathcal{Y}_{l_1^\tau l_2^\tau JI}(\hat{\Omega}_1^{\tau(\text{body})},\hat{\Omega}_2^{\tau(\text{body})}). \tag{27}$$

Here, $\hat{\Omega}_1^\tau = (\theta_1^\tau,\phi_1^\tau)$, $\hat{\Omega}_2^\tau = (\theta_2^\tau,\phi_2^\tau)$ are the orientation angles of vectors ρ_1 and ρ_2 for the τ arrangement. Superscript (body) indicates that these angles are measured in the body

frame. From the body-frame geometry defined in figure 2, $\phi_1^{\beta(\text{body})} = 0$, $\phi_1^{\gamma(\text{body})} = \pi$, $\phi_2^{\beta(\text{body})} = \pi$, $\phi_2^{\gamma(\text{body})} = \pi$ and equation (27) can be rewritten as:

$$\mathcal{Y}_{l_1^\tau l_2^\tau JM_J}(\hat{\Omega}_1^\tau, \hat{\Omega}_2^\tau) = \sqrt{\frac{16\pi^2}{2J+1}} \sum_l^J \frac{\tilde{D}^J_{IM_J}(\omega_1, \omega_2, \omega_3)}{1+(\sqrt{2}-1)\delta_{I0}} \sum_m \langle l_1^\tau m l_2^\tau I - m | JI\rangle \times Y_{l_1^\tau m}(\theta_1^{\tau(\text{body})}, \pi\delta_{\tau\gamma}) Y_{l_2^\tau I-m}(\theta_2^{\tau(\text{body})}, \pi). \tag{28}$$

For simplicity, we define

$$S_{Il_1^\tau l_2^\tau JM_J P}(\theta^\tau, \phi^\tau) \equiv \sqrt{\frac{16\pi^2}{2J+1}} \frac{1}{1+(\sqrt{2}-1)\delta_{I0}} \times \sum_m \langle l_1^\tau m l_2^\tau I - m | JI\rangle Y_{l_1^\tau m}(\theta_1^{\tau(\text{body})}, \pi\delta_{\tau\gamma}) Y_{l_2^\tau I-m}(\theta_2^{\tau(\text{body})}, \pi) \tag{29}$$

here, the right-hand side is dependent on θ, ϕ implicitly through $\theta_1^{\tau(\text{body})}$ and $\theta_2^{\tau(\text{body})}$.

Now that the asymptotic solutions are also expressed in the body-frame, the matching condition (26) becomes

$$\frac{\sum_{\mu I}\sum_{\sigma=1}^N H_\sigma^\lambda F_{\mu I}^{(\sigma)}(R_0)\Phi_{\mu I}(R_0;\theta,\phi)\tilde{D}^J_{IM_J}(\omega_1,\omega_2,\omega_3)}{R_0^{5/2}\sin\phi\cos\phi} = \sum_{i=1}^N \varphi_i(\rho_1^\tau)\left[f_\lambda(\rho_2^\tau)\delta_{i\lambda} - g_i(\rho_2^\tau)K_{i\lambda}\right] \times \frac{\sum_I \tilde{D}^J_{IM_J}(\omega_1,\omega_2,\omega_3) S_{Il_1^\tau l_2^\tau JM_J P}(\theta^\tau,\phi^\tau)}{R_0^2\cos\phi^\tau\sin\phi^\tau\mu^2/\mu_1^\tau\mu_2^{\tau\,1/2}}. \tag{30}$$

Note that the θ, ϕ angles on the left-hand side are given in α-set coordinates, and the same angles on the right-hand sides are either in the β-set or γ-set coordinates. Since the functions $\Phi_{\mu I}\tilde{D}^J_{IM_J}$ are orthogonal and normalized, we obtain the following relation,

$$\sum_{\sigma=1}^N H_\sigma^\lambda F_{\mu I}^{(\sigma)}(R_0) = R_0^{5/2}\int (\sin\phi\cos\phi)\Phi_{\mu I}(R_0;\theta,\phi)\tilde{D}^J_{IM_J}\psi_A^{(\lambda)}(\rho_1,\rho_2)\,|_{R=R_0}\,\mathrm{d}\phi\mathrm{d}\hat{\Omega} \equiv R_0^{1/2}\left(J_{\mu I}^\lambda - \sum_{i=1}^N N_{\mu I}^i K_{i\lambda}\right) \tag{31}$$

where

$$J_{\mu I}^\lambda = \int \frac{\sin\phi\cos\phi}{\sin\phi^\tau\cos\phi^\tau\mu^2/\mu_1^\tau\mu_2^{\tau\,1/2}}\Phi_{\mu I}(R_0;\theta,\phi)\varphi_\lambda(\rho_1^\tau)f_\lambda(\rho_2^\tau)S_{Il_1^\tau l_2^\tau JM_J P}(\theta^\tau,\phi^\tau)\sin\theta\mathrm{d}\theta\mathrm{d}\phi \tag{32}$$

and

$$N_{\mu I}^i = \int \frac{\sin\phi\cos\phi}{\sin\phi^\tau\cos\phi^\tau\mu^2/\mu_1^\tau\mu_2^{\tau\,1/2}}\Phi_{\mu I}(R_0;\theta,\phi)\varphi_i(\rho_1^\tau)g_i(\rho_2^\tau)S_{Il_1^\tau l_2^\tau JM_J P}(\theta^\tau,\phi^\tau)\sin\theta\mathrm{d}\theta\mathrm{d}\phi. \tag{33}$$

Equation (31) can also be expressed in matrix form

$$\mathbf{FH} = R_0^{1/2}[\mathbf{J} - \mathbf{NK}]. \tag{34}$$

Similarly, by requiring that the derivative of the wavefunction with respect to R be continuous at R_0, we obtain an equation similar to (34),

$$\mathbf{F'H} = R_0^{1/2}[\mathbf{J'} - \mathbf{N'K}] \tag{35}$$

where

$$J_{\mu l}^{\lambda l'} = \int \frac{\sin\phi\cos\phi\Phi_{\mu l}(R_0;\theta,\phi)}{\sin\phi^{\tau}\cos\phi^{\tau}} \left(\sqrt{\frac{\mu_2^{\tau}}{\mu}}\cos\phi^{\tau}\varphi_{\lambda}'(\rho_1^{\tau})f_{\lambda}(\rho_2^{\tau}) + \sqrt{\frac{\mu_1^{\tau}}{\mu}}\sin\phi^{\tau}\varphi_{\lambda}(\rho_1^{\tau})f_{\lambda}'(\rho_2^{\tau})\right)_{R=R_0} S_{ll_1^{\tau}l_2^{\tau}JM_JP}(\theta^{\tau},\phi^{\tau})\sin\theta\,\mathrm{d}\theta\,\mathrm{d}\phi + \frac{J_{\mu l}^{\lambda}}{2R_0} \tag{36}$$

and

$$N_{\mu l}^{il'} = \int \frac{\sin\phi\cos\phi\Phi_{\mu l}(R_0;\theta,\phi)}{\sin\phi^{\tau}\cos\phi^{\tau}} \left(\sqrt{\frac{\mu_2^{\tau}}{\mu}}\cos\phi^{\tau}\varphi_i'(\rho_1^{\tau})g_i(\rho_2^{\tau}) + \sqrt{\frac{\mu_1^{\tau}}{\mu}}\sin\phi^{\tau}\varphi_i(\rho_1^{\tau})g_i'(\rho_2^{\tau})\right)_{R=R_0} S_{ll_1^{\tau}l_2^{\tau}JM_JP}(\theta^{\tau},\phi^{\tau})\sin\theta\,\mathrm{d}\theta\,\mathrm{d}\phi + \frac{N_{\mu l}^{i}}{2R_0}. \tag{37}$$

After defining the log-derivative matrix

$$\mathbf{Y} = \mathbf{F'F^{-1}} \tag{38}$$

and from equations (34) and (35), we finally obtain the K matrix

$$\mathbf{K} = [\mathbf{YN} - \mathbf{N'}]^{-1}[\mathbf{YJ} - \mathbf{J'}]. \tag{39}$$

From the K matrix, the partial cross section is

$$\sigma_{ij}^{(J)} = \frac{4\pi(2J+1)}{k^2}\left|\frac{K}{1-iK}\right|_{ij}^2 \tag{40}$$

with k as the positron incident momentum.

3. Results and discussion

3.1. The s-wave

The s-wave elastic and positronium formation cross sections within the Ore gap are shown in figure 4. The results from the present calculation are shown as open triangles connected by a full line. We compare our results with the variational calculations by Brown and

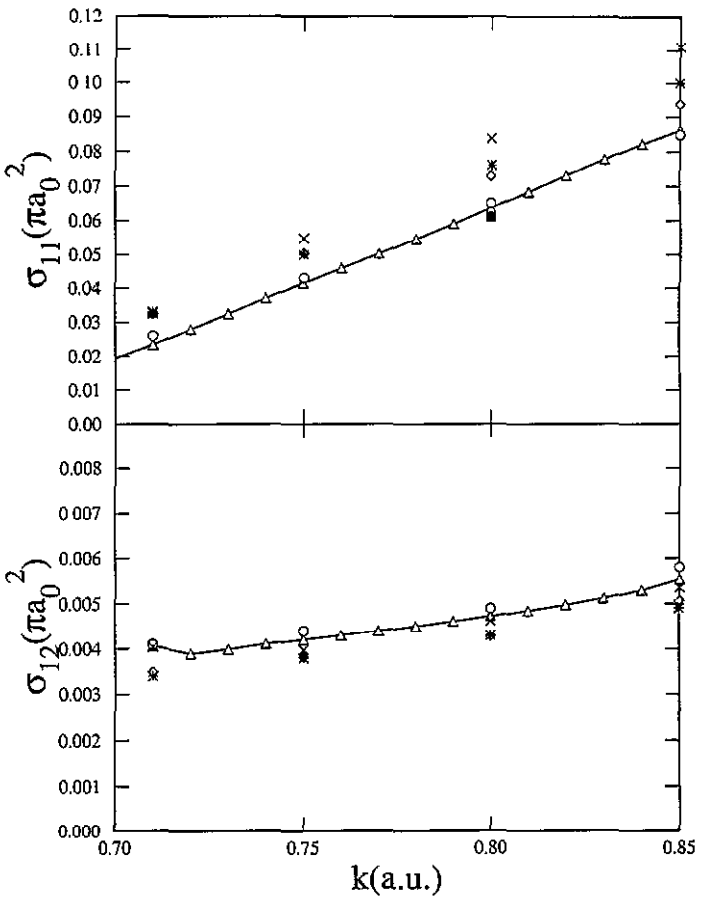

Figure 4. The s-wave elastic and positronium formation cross sections with respect to the incident wavenumber of positron in the Ore Gap. Full line and triangles, present results; open circles, Brown and Humberston (1985); diamonds, Mitroy (1993); crosses, Igarashi and Toshima (1994); asterisks, Archer *et al* (1990); full square, Winick and Reinhardt (1978).

Humberston (1985) (shown as open circles) which are considered to be the most accurate in this energy region. In the figure we also show two other calculations using hyperspherical coordinates: one from the earlier work of Archer *et al* (1990) (as asterisks), and the other from the more recent one by Igarashi and Toshima (1994) (as crosses). For results from the close-coupling method, we only show the most recent one by Mitroy (1993) (as diamonds). We also show the results by Winick and Reinhart (1978) where they used the so-called moment T-matrix method to calculate the elastic cross section and the total cross section. In the Ore gap region, the difference of the two is the positronium formation cross section. Their results for the elastic cross section are shown as full squares. Since the positronium formation cross section is small for the s-wave scattering, their results are not as accurate and are not shown.

It appears that our results agree best with the variational calculations. The differences among the hyperspherical approaches should be attributed mostly to the numerical accuracy since the methods are basically identical. The work of Archer *et al* used a different set of hyperspherical angles and a lower order FEM method was used in solving the adiabatic equation (17) at each fixed hyperradius. The work of Igarashi and Toshima differs from

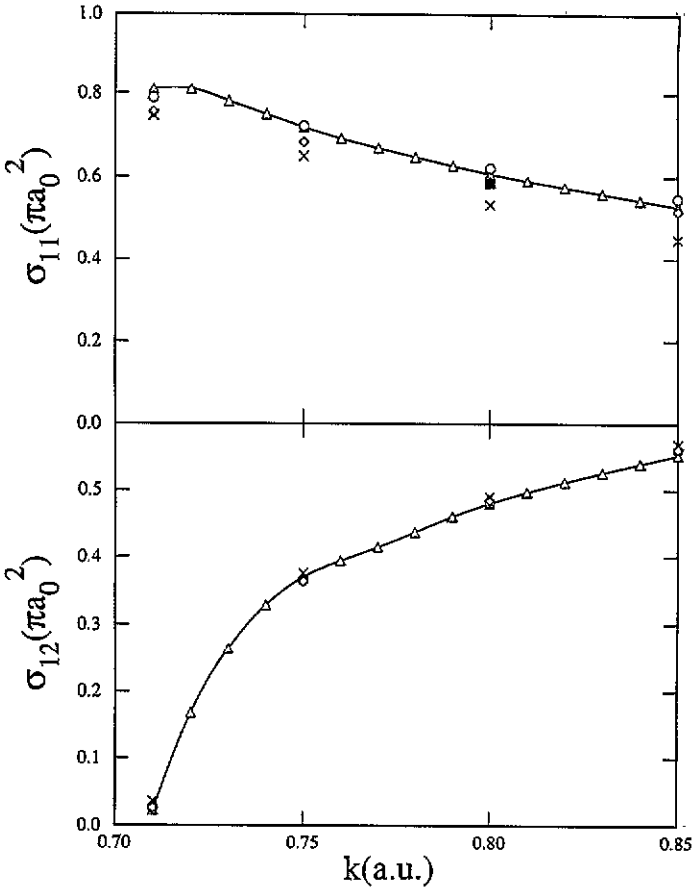

Figure 5. As in figure 4, but for the p-wave.

ours in that they used wavefunctions in the laboratory-fixed frame and the wavefunctions and potential curves at a given hyperradius were obtained by diagonalizing the Hamiltonian using Slater orbitals constructed from the β and γ (see figure 1) arrangements. The number of channels used in the calculation in the inner region is also different. In our calculation, we include 20 channels, and the matching to the asymptotic region is carried out at $R = 29.93$. We have checked the calculations by varying the matching radius and the number of channels and the results are stable to better than 2–5%. Mitroy (1993) used the close-coupling method. As noted by Igarashi and Toshima, the non-local potential between the two arrangements makes it difficult to include many bases.

It is appropriate to make comments on the matching radius chosen in our calculation. We believe that this contributes to the discrepancies among the HSCC calculations. We have varied the matching radius around $R = 29.93$ and found stable results. Our matching radius is far less than the $R = 120$ used by Archer *et al* and the $R = 400$–500 used by Igarashi and Toshima (1994). We argue that it is not appropriate to do the matching at such large distances unless the number of channels in the inner region is increased correspondingly. It is desirable to view the hyperspherical close coupling method as a variation of the R-matrix method. The number of channels used in the inner region is supposed to represent the 'exact' solution in the inner region which is often done in the R-matrix method by expanding into a large basis set. If the matching radius is increased, the number of basis

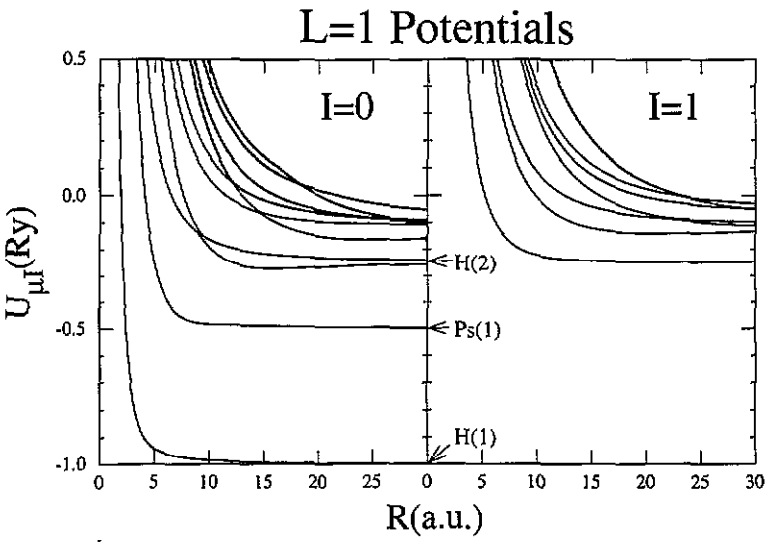

Figure 6. Potential curves for the p-wave with ten channels for $I = 0$ and seven channels for $I = 1$. The dissociation states at large R are also indicated. The third and fourth lowest channels for $I = 1$ converge to the $n = 3$ excited states of H. The highest three channels for $I = 1$ converge to the $n = 4$ excited states of H atom. Note that the higher potential curves have not reached the asymptotic limits at $R = 30$.

functions has to be increased. Similarly, if the matching radius is increased in the HSCC method, the number of channel functions should be increased as well. Assuming that we have neglected the polarization potential from $R = 29.93$ to infinity, we have estimated that the error in the elastic phaseshift is of the order of a fraction of 1%.

We do not show results from other earlier calculations in figure 4. Results from other close coupling calculations were summarized by Mitroy (1993) and the earlier results have been discussed in the review by Humberston (1986).

3.2. The p-wave

The p-wave elastic and positronium formation cross sections are shown in figure 5. We compare the results with the variational calculations by Brown and Humberston (1985), the close-coupling calculation by Mitroy (1993), the hyperspherical results of Igarashi and Toshima (1994) and those from Winick and Reinhardt (1978). For the elastic cross section, our results agree very well with those of Brown and Humberston. For the positronium formation cross sections, our results are in good agreement with those of Brown and Humberston. Results from the other three calculations are also all in reasonable agreement, especially at low energies.

In this calculation we included twenty channels. The lowest 17 potential curves are shown in figure 6, ten for $I = 0$ and the other seven for $I = 1$. Recall that I is the magnitude of the projection of the total angular momentum along the body-frame z' axis. For $I = 0$, the two lowest curves converge to the ground state of atomic hydrogen and of the positronium, respectively. The two pairs of higher curves converge to the $n = 2$ excited states of hydrogen and of the positronium, respectively. For $I = 1$, the two lowest curves converge to the $n = 2$ excited states. These curves are similar to molecular potential curves where R is the internuclear distance, and $I = 0$ curves correspond to the σ curves and $I = 1$ to the π curves. The potential curves shown above are not adiabatic curves since the coupling between the different I components is not included. We have found

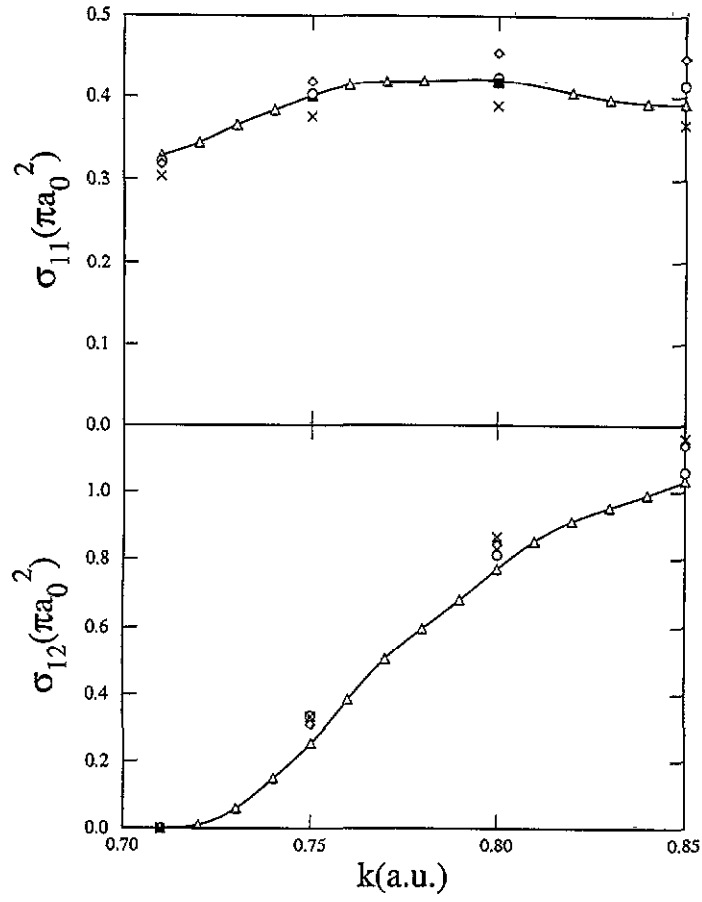

Figure 7. As in figure 4, but for the d-wave.

that the inclusion of these couplings quite important. In a test calculation, we demonstrated that failure to include the rotational coupling results in much smaller positronium formation cross sections.

3.3. The d-wave

The d-wave elastic and positronium formation cross sections are shown in figure 7. For the elastic cross section, our results agree very well with the results of Brown and Humberston (1985). The results from Igarashi and Toshima (1994) are slightly lower and those of Mitroy (1993) are slightly higher, and the only point from Winick and Reinhardt (1978) is right on our curve. For the positron formation cross section, we agree again very well with those from Brown and Humberston (1985), and those by Igarashi and Toshima and by Mitroy are slightly higher.

In our calculation, we include 14 channels, six for $I = 0$, four for $I = 1$, and four for $I = 2$.

3.4. The f-wave

The f-wave results for elastic and positronium formation cross sections are shown in figure 8. There are no variational results to compare with except for the result from Winick and

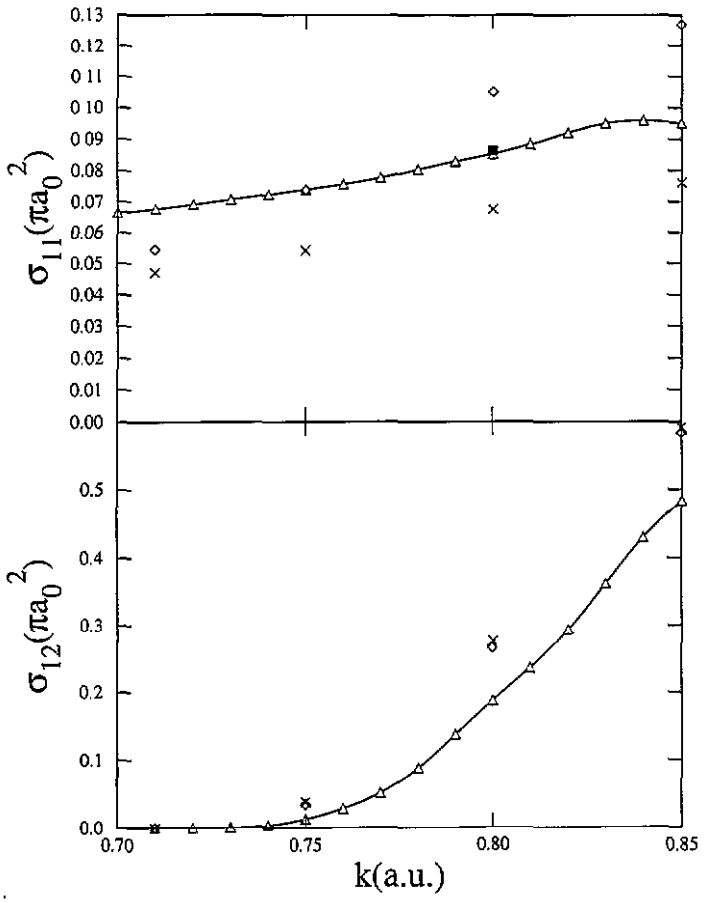

Figure 8. As in figure 4, but for the f-wave.

Reinhardt which agrees with ours. For elastic cross sections, the results of Igarashi and Toshima are about 20% smaller than ours, and those by Mitroy are about 20% higher than ours at higher energies. For positron formation cross sections, the results by Igarashi and Toshima and by Mitroy agree with each other but they are higher than our results by about 20% at higher energies.

The larger discrepancies for the f-wave may be an indication of the convergence of the calculation. We agree with Winick and Reinhard at $k = 0.8$. Since their results at this energy for $J = 1$ and 2 are essentially identical to the variational results of Brown and Humberston, we may be able to feel confident of the values we have calculated for the f-wave. Note that the computing time increases quickly for the higher partial wave. We used 18 channels for the f-wave calculation, six for $I = 0$ and four each for $I = 1$, 2 and 3.

We have not extended the calculations to higher partial waves. Such calculations can be easily done, but it would take more computer time. To obtain total positronium formation cross sections one can use the results from Winick and Reinhardt or from Igarashi and Toshima for the higher partial waves. Or when such a need arises, the present method can be extended to these higher partial waves.

4. Conclusion

We have applied the hyperspherical close coupling method to obtain elastic and positronium formation cross sections in positron–atomic hydrogen collisions in the Ore gap energy region. We have performed calculations for $J = 0$, 1, 2 and 3, and showed that the results obtained are of comparable accuracy to those obtained by the variational method. In the variational calculations, parameters of the order of hundreds are used and the parameters have to be varied for each J. In contrast, the hyperspherical close coupling method is a direct solution of the scattering problems.

Our results show that the hyperspherical close coupling method can be used to treat direct and rearrangement collisions involving three charged particles. Despite that there are no experimental data in existence for the present positron–atomic hydrogen collision system, the elaborate variational calculations for this system provide accurate data which allow us to test the present general method. The good agreement of the present results with these variational calculations illustrates that the hyperspherical close coupling method not only can be applied to atomic systems such as H^- and He, but now has been extended to rearrangement collisions. One important ingredient in carrying out the hyperspherical close-coupling calculation is that the potential curves and the coupling terms should be calculated accurately. We have used the higher-order finite-element method to obtain accurate potential curves and coupling terms.

The present method is very general. We are extending the calculations to include more channels so that excitation to the $n = 2$ states of atomic hydrogen and positronium formation to the $n = 2$ excited states can be obtained. The present method is also written for general three-body systems where the masses and charges in the system can be varied simply as input parameters, and the potentials between the particles can be modified to any local potentials. Currently we are extending this approach to treat these problems.

Acknowledgments

This work was supported in part by the US Department of Energy, Office of Energy Research, Office of Basic Energy Sciences, Division of Chemical Sciences. The calculations using the FEM were conducted using the resources of the Cornell Theory Center, which receives major funding from the National Science Foundation and IBM Corporation, with additional support from the New York State Science and Technology Foundation and members of the Corporate Research Institute. We also would like to thank Professor Janine Shertzer who is always so eager to help us on the finite element method. Without her continuing assistance this project would have taken a much longer time to carry out.

References

Archer B J, Parker G A and Pack R T 1990 *Phys. Rev.* A **41** 1303
Basu M, Mukherjee M and Ghosh A S 1989 *J. Phys. B: At. Mol. Opt. Phys.* **22** 2195
Bathe K and Wilson E 1976 *Numerical Methods of Finite Element Analysis* (Englewood Cliffs, NJ: Prentice-Hall)
Bhatia A K and Temkin A 1964 *Rev. Mod. Phys.* **36** 1050
Brown C J and Humberston J W 1985 *J. Phys. B: At. Mol. Phys.* **18** L401–6
Cavagnero M, Zhen Z and Macek J 1990 *Phys. Rev.* A **41** 1225
Chen Z and Lin C D 1990 *Phys. Rev.* A **42** 18
Delves L M 1959 *Nucl. Phys.* **9** 391
—— 1962 *Nucl. Phys.* **20** 268

DeVries K M, Bartschat K, McEachran R P and Stauffer A D 1993 *Proc. 18th Int. Conf. on Physics of Electronic and Atomic Collisions* ed ? (Amsterdam: North-Holland) Abstracts p 410
Hewitt R N, Noble C J and Bransden B H 1990 *J. Phys. B: At. Mol. Opt. Phys.* **23** 4185
Humberston J W 1986 *Adv. At. Mol. Phys.* **22** 1
Humberston J W and Armour E A G 1987 *Atomic Physics With Positrons* (New York: Plenum)
Igarashi A and Toshima N 1994 *Phys. Rev.* A **50** 232
Kadomtsev M B and Vinitsky S I 1987 *J. Phys. B: At. Mol. Phys.* **20** 5723
Kwan C K, Zhou S, Kauppila W E, Parikh S P and Stein T S 1993 *Proc. 18th Int. Conf. on Physics of Electronic and Atomic Collisions* (Amsterdam: North-Holland) Abstracts p 430
Landau L D and Lifshitz E M 1977 *Quantum Mechanics* 3rd edn (Oxford: Pergamon)
Launay J M 1990 *Chem. Phys. Lett.* **169** 473
Launay J M and Le Dourneuf M 1989 *Chem. Phys. Lett.* **163** 178
Lin C D 1984 *Phys. Rev.* A **29** 1019
—— 1986 *Adv. At. Mol. Phys.* **22** 77
Lin C D and Liu X H 1988 *Phys. Rev.* A **37** 2749
Liu G and Gien T T 1992 *Phys. Rev.* A **46** 3918
Liu X H, Chen Z and Lin C D 1991 *Phys. Rev.* A **44** 5468
Mitroy J 1993 *J. Phys. B: At. Mol. Opt. Phys.* **26** 4861
Shertzer J and Levin F S 1991 *Phys. Rev.* A **43** 2531
Smith F T 1960 *Phys. Rev.* **120** 1058
Sperber W, Becker D, Raith W, Schwab A, Sonapius G, Spicher G and Weber M 1992 *Phys. Rev. Lett.* **68** 3690
Stein T S, Kauppila W E, Kwan C K and Zhou S 1993 *Proc. 18th Int. Conf. on Physics of Electronic and Atomic Collisions* (Amsterdam: North-Holland) Abstracts p 416
Tang J Z, Watanabe S and Matsuzawa M 1992a *Phys. Rev.* A **46** 2437
Tang J Z, Watanabe S, Matsuzawa M and Lin C D 1992b *Phys. Rev. Lett.* **69** 1633
Winick J R and Reinhardt W P 1978 *Phys. Rev.* A **18** 925
Zhou B, Lin C D ,Tang J Z, Watanabe S, Matsuzawa M 1993a *J. Phys. B: At. Mol. Opt. Phys.* **26** 2555
Zhou S, Kauppila W E, Kwan C K and Stein T S 1993b *Proc. 18th Int. Conf. on Physics of Electronic and Atomic Collisions* (Amsterdam: North-Holland) Abstracts p 415
Zhou Y and Lin C D and Shertzer J 1993c *J. Phys. B: At. Mol. Opt. Phys.* **26** 3937